Thermochronology of the Needle Falls Shear Zone: A post-collisional high-strain zone of the Trans-Hudson Orogen

Article *in* Canadian Journal of Earth Sciences · February 2011

DOI: 10.1139/e03-033

CITATIONS
7

READS
37

4 authors, including:

John Fedorowich

24 PUBLICATIONS **374** CITATIONS

SEE PROFILE

Mel R. Stauffer

University of Saskatchewan

54 PUBLICATIONS **1,171** CITATIONS

SEE PROFILE

Thermochronology of the Needle Falls Shear Zone: a post-collisional high-strain zone of the Trans-Hudson Orogen

John S. Fedorowich, Mel R. Stauffer, Rob Kerrich, and John F. Lewry

Abstract: The Needle Falls Shear Zone is a major Paleoproterozoic discontinuity separating an Archean craton from accreted Paleoproterozoic terranes in the western Trans-Hudson Orogen. It is a 1 km-wide subvertical mylonite zone forming the southwestern sector of a northeast-trending shear system extending for more than 400 km. Kinematic data indicate oblique, east-side-up dextral strike-slip displacement throughout its evolution from ductile through late brittle deformation. For most of its exposed length, it marks the northwestern margin of the Wathaman Batholith. The oldest Pb-evaporation ages of zircons from mylonite average 1857 Ma, consistent with published zircon ages of the Wathaman Batholith, confirming the batholith is protolith for much of the shear zone. The synkinematic metamorphic assemblage of amphibole–biotite–quartz–feldspar signifies deformation under amphibolite-facies conditions (500–630°C). Oxygen isotope fractionations between quartz–hornblende and quartz–biotite pairs in textural equilibrium give temperatures from 430°C to 610°C, with a mode at 550°C. For hornblende–biotite pairs, $^{40}Ar/^{39}Ar$ plateau ages of hornblende cluster at 1780 Ma and of biotite at 1757 Ma. Given textural and oxygen isotope equilibrium between hornblende, biotite, and quartz, these ages are interpreted as cooling ages; consequently, this sector of the Trans-Hudson Orogen cooled from 500°C to 300–350°C over about 23 million years following ductile deformation. The timing of ductile deformation cannot be well constrained, but occurred after emplacement of the Wathaman Batholith at 1857 Ma and prior to cooling of amphibole below its Ar blocking temperature at 1780 Ma.

Résumé : La zone de cisaillement de Needle Falls est une discontinuité majeure (Paléoprotérozoique) séparant un craton archéen de terranes paléoprotérozoiques accrétés dans l'ouest de l'orogène trans-hudsonien. Il s'agit d'une zone de mylonite de 1 km de large, sub-verticale, formant le secteur sud-ouest d'un système de cisaillement de direction NE, s'étendant sur plus de 400 km. Les données cinématiques indiquent un déplacement oblique, à décrochement dextre, avec le coté est vers le haut durant son évolution de déformation ductile précoce à cassante tardive. La plus grande partie qui affleure marque la bordure nord-ouest du batholite de Wathaman. Les âges les plus vieux, déterminés par évaporation Pb sur des zircons provenant de la mylonite, ont une moyenne de 1857 Ma, ce qui concorde avec les données publiées d'âges de zircons du batholite de Wathaman, confirmant que le batholite est un protolithe pour une grande partie de la zone de cisaillement. L'assemblage métamorphique syn-cinématique d'amphibole–biotite–quartz– feldspath signifie une déformation sous les conditions de faciès des amphibolites (500 à 630 °C). La séparation des isotopes de l'oxygène entre les paires quartz-hornblende et quartz-biotite en équilibre textural donne des températures de 430 à 610 °C avec une valeur modale à 550 °C. Pour les paires hornblende-biotite, les âges du plateau $^{40}Ar/^{39}Ar$ de la hornblende forment des ensembles à 1780 Ma et à 1757 Ma pour la biotite. Étant donné l'équilibre de la texture et des isotopes de l'oxygène entre la hornblende, la biotite et le quartz, ces âges sont interprétés comme étant des âges de refroidissement; par conséquent, ce secteur de l'orogène trans-hudsonien a refroidi de 500 à 300–350 °C durant une période d'environ 23 millions d'années après la déformation ductile. Le moment de la déformation ductile ne peut pas être bien cerné, mais il a eu lieu après la mise en place du batholite de Wathaman vers 1857 Ma et avant le refroidissement de l'amphibole sous la température de blocage de l'Ar à 1780 Ma.

[Traduit par la Rédaction]

Received 26 November 2002. Accepted 26 February 2003. Published on the NRC Research Press Web site at http://cjes.nrc.ca on 6 August 2003.

Paper handled by Associate Editor M. St-Onge.

John S. Fedorowich. FNX Mining Company Inc., 1300 Kelly Lake Road, Sudbury, ON P3E 5P4, Canada.
Mel R. Stauffer[1] and Rob Kerrich. Department of Geological Sciences, University of Saskatchewan, Saskatoon, SK S7N 5E2, Canada.
John F. Lewry.[2] Geology Department, University of Regina, Regina, SK S4S 0A2, Canada.

[1]Corresponding author (e-mail: mel.stauffer@usask.ca).
[2]Deceased.

 doi: 10.1139/E03-033

Introduction and scope

The Needle Falls Shear Zone (NFSZ) is a major, mainly ductile (mylonitic), structural element in the tectonic architecture and evolution of the Paleoproterozoic Trans-Hudson Orogen (THO; Fig. 1). For most of its > 400 km length, it separates reworked Archean continental crust of the Hearne Province, and its partial cover of inboard supracrustal Wollaston Group rocks to the west, from the ca. 1857 Ma Wathaman Batholith and other accreted, juvenile, Paleoproterozoic arc components of the Reindeer Zone to the east. The NFSZ splays at its northwest end into the Parker Lake (PLSZ) and Reilly Lake (RLSZ) shear zones, near whose junction the Wathaman River area of this study is located (Fig. 1; Stauffer 1984; Lewry and Collerson 1990).

Interpretation of Lithoprobe seismic reflection profiles suggests that the NFSZ can be traced to a depth of about 18 km, where it has a moderate westerly dip and appears either to merge with, or be truncated by, a series of gently west-dipping structures (Lucas et al. 1993; Hajnal et al. 1996). According to Jones et al. (1993), the western boundary of the North American Central Plains conductivity anomaly is also delimited by the NFSZ.

The Wathaman Batholith was emplaced between 1865 and 1850 Ma, and collision of this sector of the THO with the Superior Province completed by 1790 Ma. (Bickford et al. 1990; Meyer et al. 1992; Ansdell et al. 1995). Accordingly, the $^{40}Ar/^{39}Ar$ dating of synkinematic hornblende and biotite in both mylonite and crosscutting veins of the NSFZ may further constrain the age of displacement and thermochronology along this major orogen-parallel shear zone during late accretion within the THO. Documenting the development of structural fabrics, metamorphic mineral growth, and vein history are essential for selecting minerals for geochronological study and for interpretion of the results. $^{40}Ar/^{39}Ar$ ages may represent cooling through the blocking temperature or resetting below blocking temperatures by deformation or fluid events (McDougall and Harrison 1988; Kerrich and Cassidy 1994). Radiogenic isotope systems are typically reset by dynamic recrystallization, a major ductile deformational process, or static recrystallization during recovery (Brodie and Rutter 1985; Passchier and Trouw 1996).

The chance of successfully dating kinematic events is increased by coordinated use of a number of independent methods. The general approach used here to obtain ages of deformational fabrics is similar to that outlined by Gromet (1991) and includes (1) field and petrographic identification of the fabrics to be dated; (2) verification that the minerals in the rock have undergone dynamic recrystallization; and (3) radiogenic isotope analysis of as many phases as is practicable. Refinements to this approach include the use of electron micrprobe back-scattered electron (BSE) image analysis and wavelength dispersive spectrometry (WDS) to confirm the homogeneity of target minerals. These methods can detect potentially problematic mineral intergrowths down to the micrometre scale. A further refinement involves the use of stable oxygen isotopes to establish if anions are in equilibrium among the minerals of a particular assemblage. Anion equilibrium of a mineral indicates that the cations have not been significantly disturbed since crystallization, and therefore lends further confidence that the mineral specimen will ultimately provide a meaningful age. This approach may also provide constraints on the thermal history of the rock during deformation.

Characteristics of the Needle Falls Shear Zone

The kinematic evolution of the NFSZ has been studied previously at the Needle Falls study area by Stauffer and Lewry (1988, 1993; Fig. 2, location 1), from which the following description is summarized. The shear zone is ~ 1.2 km wide, maintains a consistent north-northeast strike, and has a subvertical dip (Fig. 2). It is developed mainly in rocks of the Paleoproterozoic Wathaman Batholith, but a 30 m-wide strip along the northwestern side is developed in granite of the Archean Hearne Craton. It can be subdivided into three subzones displaying progressively more intense deformation to the northwest: zone 1, ultramylonite; zone 2, mylonite; and zone 3, protomylonite (Stauffer and Lewry 1993). The body of this paper is concerned with the bulk of the NFSZ that was derived from rocks of the Wathaman Batholith. The northwestern component developed in Hearne Craton rocks was not well studied.

Structural fabrics

Within the shear zone, mylonites exhibit numerous ductile to brittle features, including (1) flaser structure defined by deformed original grains and new metamorphic mineral growth C fabric, with local C–S fabrics); (2) winged porphyroclasts (rarely pressure shadows), mainly symmetric but δ-type is common; (3) gently plunging stretching lineation (L); (4) compressional and extensional microfaults ranging from thin ductile shear bands to late brittle faults; (5) asymmetric boudins; (6) early isoclinal and sheath folds; (7) later asymmetric folds related to compressional microfaults; and (8) variably rotated, sigmoidal, and folded veins of quartz, or, less commonly, K-feldspar and hornblende ± biotite. All ductile shear-sense indicators suggest dextral displacement with a minor east-side-up component, as do most younger ductile transitional to brittle, and brittle features (Stauffer and Lewry 1993).

Vein relationships

Quartz-rich veins occur intermittently throughout the NFSZ, but are most abundant within zone 1 ultramylonites (Fig. 2). These occur both along the C-foliation and crosscutting it at various, mostly steep, angles. Veins parallel to the C-foliation are generally boudinaged to varying degrees. Oblique quartz veins occur as straight, sigmoidal, or tightly folded vein sets. Such veins and their subsequent deformation indicate ductile transitional to brittle conditions of deformation (e.g., Ramsay and Huber 1987, p. 603; Passchier and Trouw 1996).

A set of distinctive K-feldspar–quartz–hornblende–biotite–titanite veins also occur in zones 1 and 2. These crosscut the C-foliation and have pronounced centimetre-scale alteration haloes involving feldspathization and hornblende blastesis in the host rock. Some are sigmoidal, suggesting that vein growth was late synkinematic. They probably originated as extensional veins because the vein tips point approximately

Fig. 1. Location of the Needle Falls Shear Zone (NFSZ) (modified from Stauffer and Lewry 1993). Upper left inset map shows location of the Trans-Hudson Orogen (THO; dense stipple pattern) in the Canadian Shield (open stipple pattern). In Saskatchewan (Sask.), the THO includes the Hearne Province (HP), Reindeer Zone (RZ), and Wathaman Batholith (WB). It is bounded to the southeast by the Archean Superior Province (SP) and to the northwest by the Archean Rae Province (RP). Lower right inset map shows the northern Saskatchewan sector of the THO. Labels are same as in other inset map, with addition of the Snowbird "line" (SBL) or "tectonic zone," another major ductile high-strain zone, and the Mesoproterozoic Athabasca Basin (AB). In the main figure, the NFSZ splays at its northwest end into the Parker Lake (PLSZ) and Reilly Lake (RLSZ) shear zones, near whose junction the Wathaman River area of this study is located. Wollaston Domain (WD) and Peter Lake Domain (PLD, largely bounded by splays of the NFSZ) are part of the HP. RL is Reindeer Lake; and CR is Churchill River, along which the Needle Falls study area is located. Wath. Bath., Wathaman Batholith.

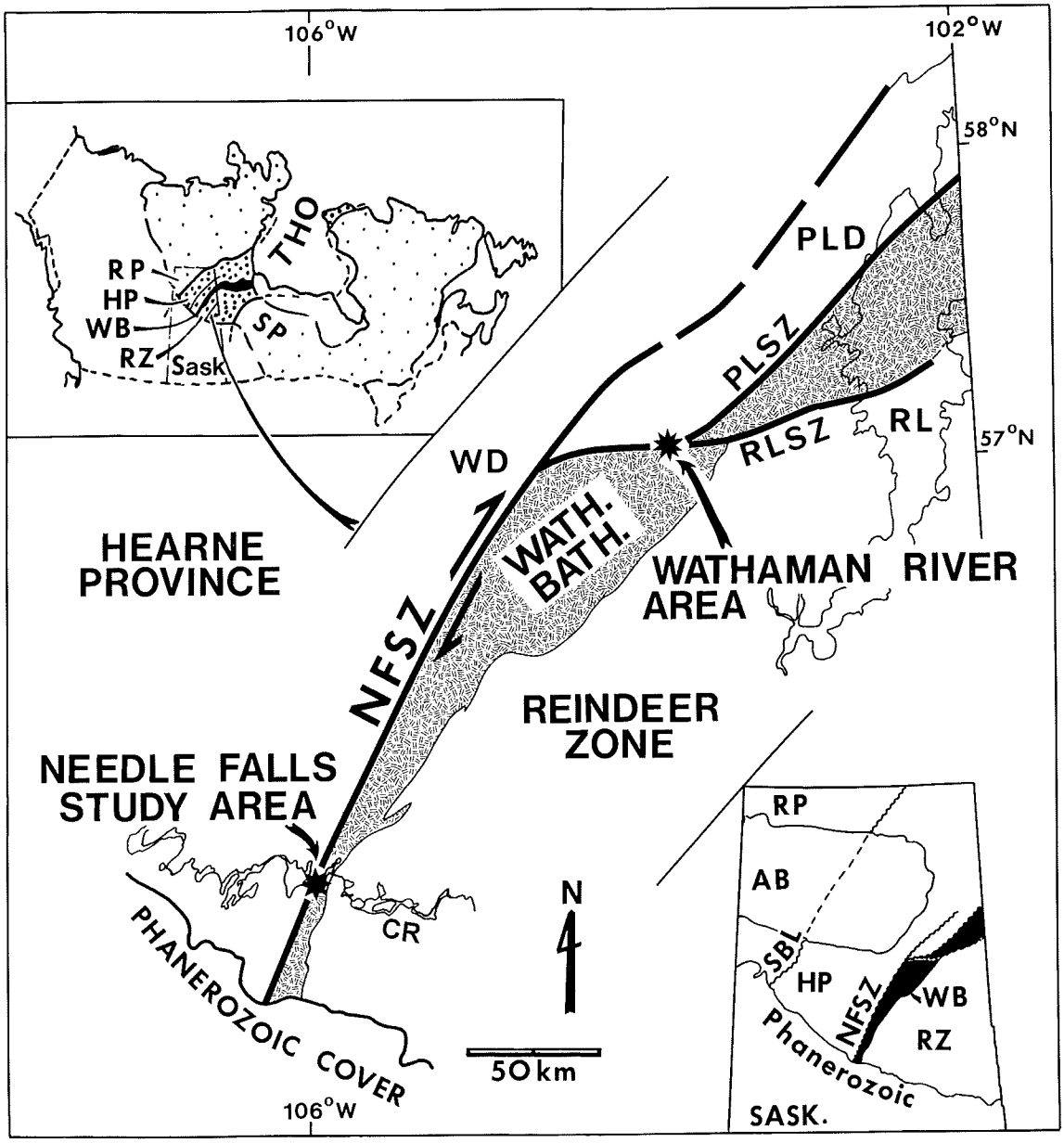

in the direction of maximum compressive stress (σ_1), as deduced from the C-foliation and its dextral slip indicators (Fig. 3*a*). Also, the tips of some of these are segmented, having been displaced incrementally along the C-foliation.

Petrography

Two phases of amphibolite-grade metamorphism resulting in the growth of hornblende and biotite were recognized: one coeval with development of the lineated mylonite's C-foliation (L–S style fabric), the other during later growth of veins and their blastesis halos.

L–S fabric

Planar- and linear-preferred dimensional orientation of quartz, feldspar, hornblende, and biotite define the lineated C-foliation (L–S) fabric. Samples #5, #10, and #16 with well-developed L-S fabrics were geochronologically analyzed using $^{40}Ar/^{39}Ar$

Fig. 2. At Needle Falls on the Churchill River the Needle Falls Shear Zone (NFSZ) is about 1.2 km wide and is subdivided into three principal zones: zone 1, ultramylonite; zone 2, mylonite; and zone 3, protomylonite. The eastern side comprises main-phase Wathaman megacrystic monzogranite–granodiorite (zone 4a) and moderately deformed Wathaman Batholith (zone 4b) with a weakly gneissic texture overprinted by shear foliation.

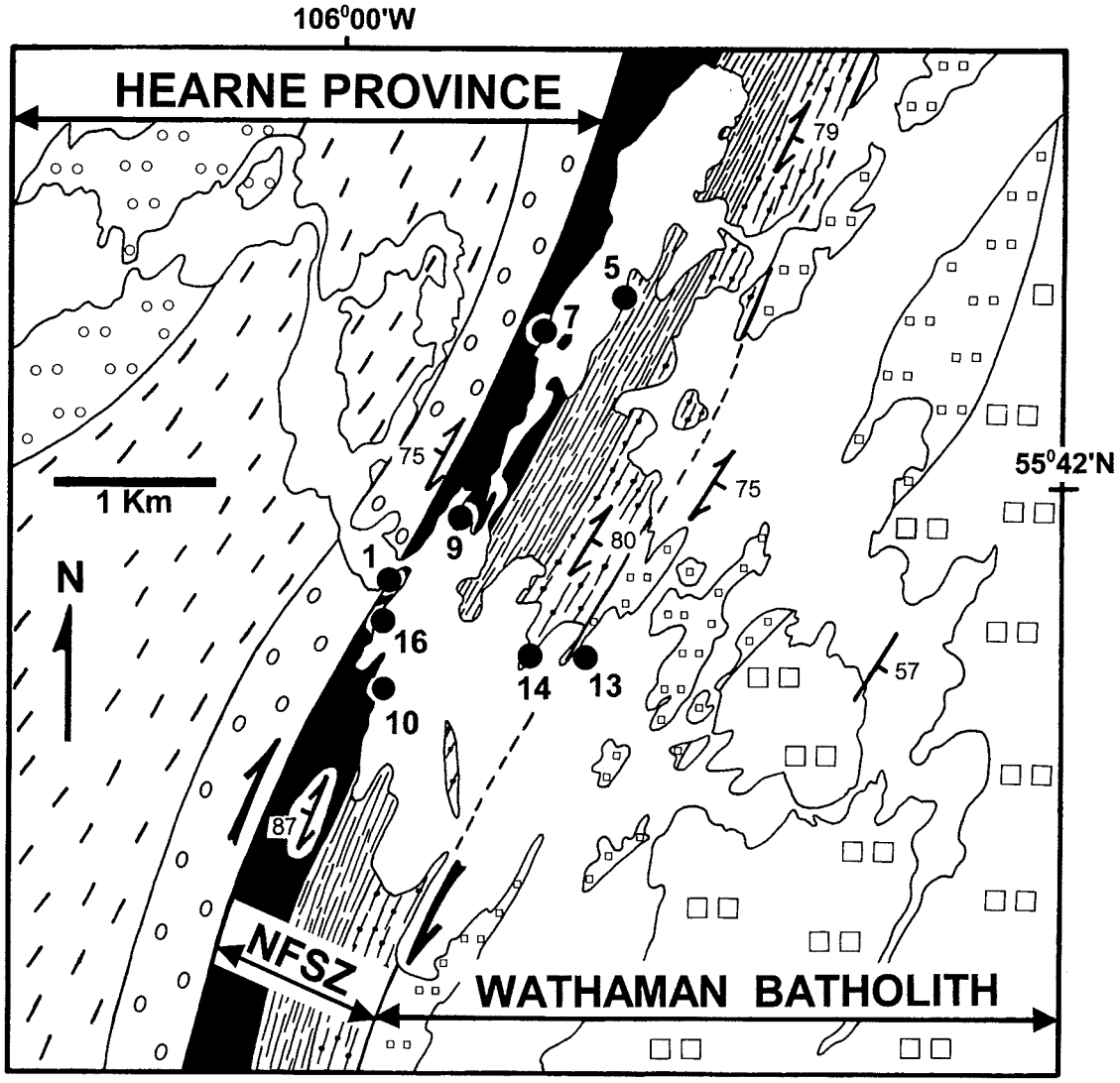

NEEDLE FALLS SHEAR ZONE

- ULTRAMYLONITE - ZONE 1
- MYLONITE - ZONE 2
- PROTOMYLONITE - ZONE 3

WATHAMAN BATHOLITH

- MEGACRYSTIC GRANITOID - ZONE 4a
- WEAKLY DEFORMED - ZONE 4b

HEARNE PROVINCE

- UNDIVIDED GRANITOID
- WOLLASTON GROUP
- ARCHEAN AUGEN GRANITE

- 75 C-FOLIATION STRIKE & DIP
- 57 GNEISSIC FOLIATION STRIKE & DIP
- 1 SAMPLE LOCATION

Fig. 3. (*a*) Field photograph of a dextral sigmoidal hornblende–plagioclase vein cutting ultramylonite. Note folding near the vein tips with the C-foliation axial planar. Photo of flat outcrop surface taken looking to the NW. Photomicrographs (*b*) to (*d*) show an *X*–*Z* section through zone 1 ultramylonite (sample site #10, Fig. 2). (*b*) Hornblende (Hb) lineation along C-foliation (plane polarized light (PPL) 15 × magnification). The inset box shows location of Fig. 3*c*. (*c*) Hornblende has incorporated small strained quartz grains, indicating syntectonic growth along the C-foliation. PPL 50 × magnification. (*d*) A high degree of dynamic recrystallization is evident in this cross-polarized view of the same area as shown in Fig. 3*c*. Polygonal quartz grains and ribbons are also highly elongate along C-foliation. Note also the very fine-grained biotite lamellae within hornblende and in the ultramylonite matrix. Photomicrographs (*e*) and (*f*) are from zone 3 (sample site # 14, Fig. 2). (*e*) Several K-feldspar porphyroclasts (P) are shown here in an *X*–*Z* section (PPL 15 × magnification). The inset box shows the location of Fig. 3*f*. (*f*) Clockwise rotation is shown by this porphyroclast, wherein the pressure shadows contain polygonal quartz–feldspar intergrown with fresh biotite and hornblende laths. The porphyroclast also contains sericite and displays strain lamellae and oblique-to-perpendicular fracture sets. PPL 50 × magnification.

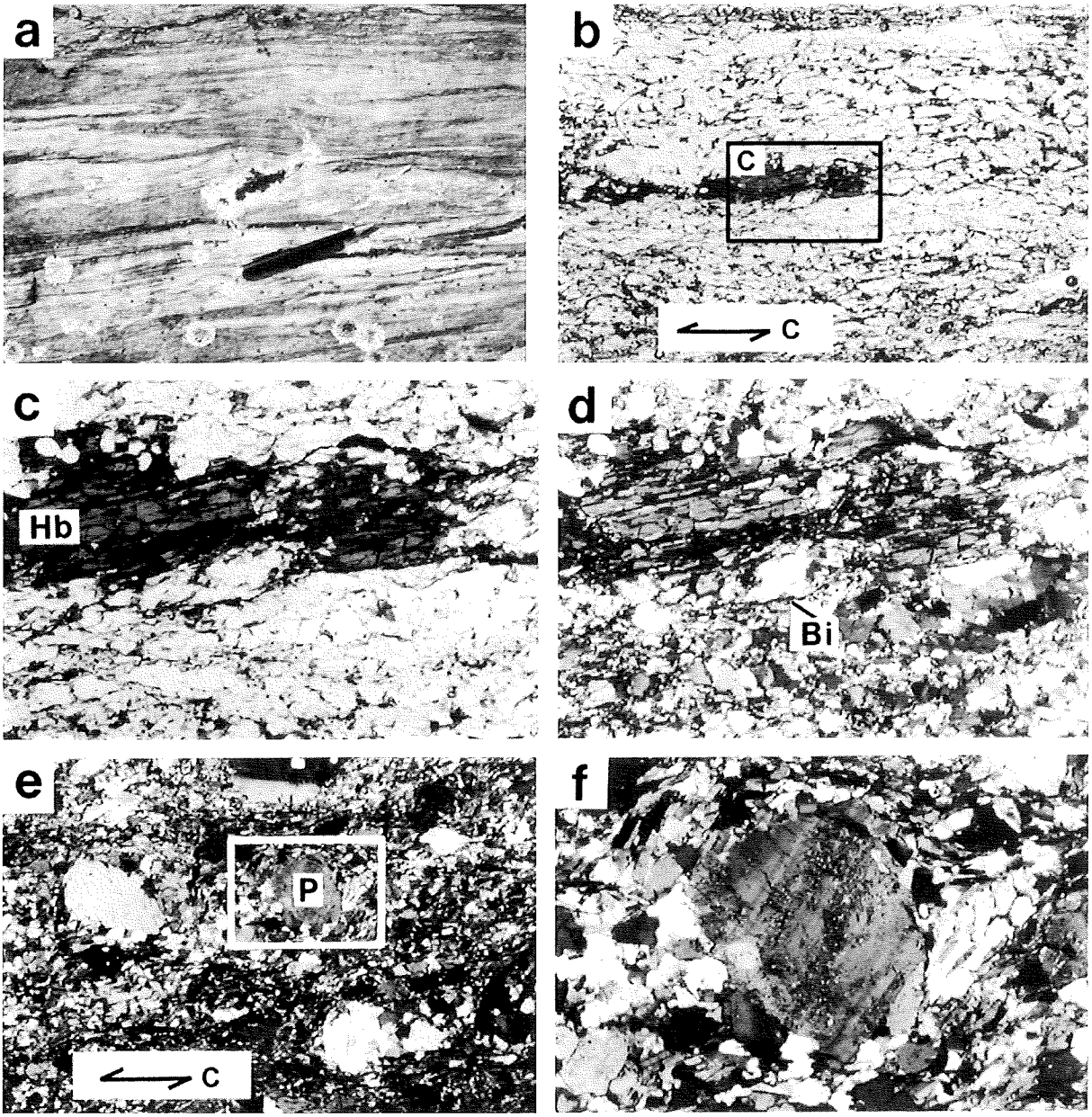

techniques (Table 1). The C-foliation is defined partly by the dimensional alignment of biotite, which comprises 10–15% of the rock, and by flattened feldspar and quartz grains (Fig. 3*b*, #10, site 8). Lineation is defined by oriented growth of hornblende and coaxial elongation of feldspar and quartz grains (Fig. 3*c*). The anhedral shape of hornblende grains, their alignment with other fabric elements (biotitic C-foliation), and their entrainment of strained quartz subgrains suggest that hornblende growth was syntectonic (Figs. 3*c*, 3*d*). The mylonite has a distinct layering defined by alternating biotite-poor and biotite-rich layers, locally intergrown with hornblende. A strain gradient is developed toward these biotitic

Table 1. Radiogenic and stable isotope results, Needle Falls Shear Zone.

Sample	Mineral	$\delta^{18}O$	Temperature (°C)	$^{40}Ar/^{39}Ar$ age (Ma)	Pb/Pb age zircon	U/Pb age titanite	Description
Needle Falls area							
#1	quartz	6.8					Protomylonite in Archean augen granitoid (zone 1)
	biotite	0.2	q-bi = 440	**1738 ± 7 bi**			
	magnetite	1.3	q-mt = 560				
#5	quartz	9.1					Mylonite (WB) with Kspar porphyroclasts
	biotite	2.9	q-bi = 460	**1732 ± 9 bi**			(zone 2)
	magnetite	1.7	q-mt = 440				
#7	quartz	8.7					Vein; Kspar-hb-bi-q; distinctive alteration halo;
	hornblende	4.4	q-hb = 550	**1791 ± 7 hb**		**1912 ± 5**	cuts C-foliation; folded (zone 1)
	biotite	3.7	q-bi = 540	**1761 ± 7 bi**			
	K-feldspar	15.5					
#9	quartz	9.8					Vein; feldspar-q-hb;
	hornblende	5.8	q-hb = 580	***1845 ± 9 hb**		**1766 ± 11**	alteration halo; cuts C-foliation (zone 1)
#10	quartz	9.4			**1856 ± 3**		Beaded mylonite (WB); laminated intermediate to
	hornblende	5.0	q-hb = 550	**1772 ± 12 hb**	**1844 ± 3**		felsic (zone 1)
	biotite	3.9	q-bi = 500		**1837 ± 11**		
	magnetite	1.2	q-mt = 550				
#13	quartz	9.6					Wathaman Batholith; moderately sheared
	hornblende	4.5	q-hb = 490	**1773 ± 11 hb**		**1774 ± 55**	(zone 4b)
	biotite	2.7	q-bi = 430	**1747 ± 8 bi**			
	magnetite	1.0	q-mt = 450				
	epidote	6.0					
#14	quartz	8.9					Mylonite (WB) with Kspar porphyroclasts and
	hornblende	5.2	q-hb = 610	**1777 ± 11 hb**	**1809 ± 14**		hornblende porphyroblasts (zone 3)
	biotite	3.6	q-bi = 520	**1761 ± 7 bi**	**1859 ± 4**		
	magnetite	0.3	q-mt = 500				
	epidote	4.9					
#16	quartz	10.0					Mylonite (WB); laminated felsic and intermediate
	hornblende	5.2	q-hb = 510	***1855 ± 10 hb**			(zone 1)
	biotite	4.2	q-bi = 490	***1906 ± 12 bi**			
	magnetite	1.2	q-mt = 520				
Wathaman River area							
#22	quartz	8.4					Mylonite (WB); Kspar porphyroclasts
	biotite	3.5	q-bi = 550	***1790 ± 11 bi**			
#24	quartz	10.2					Mylonite (WB); Kspar porphyroclasts
	hornblende	4.8	q-hb = 450	***1889 ± 18 hb**			
	biotite	3.8	q-bi = 470	***1879 ± 9 bi**			

Note: Mineral abbreviations: q,, quartz; hb,, hornblende; bi,, biotite; mt,, magnetite; Kspar,, K-feldspar. WB refers to mylonite derived from rocks of the Wathaman Batholith; *indicates an anomalous $^{40}Ar/^{39}Ar$ age. Fractionation factors of Bottinga and Javoy (1975) were used to calculate temperatures.

layers, characterized by grain-size reduction, in which 300 μm-wide layers of 20–50 μm subgrains are developed. Locally, folded quartz–feldspar veins crosscut the fabric, and rotated porphyroclasts are abundant (Figs. 3*e*, 3*f*).

Porphyroclasts of perthitic K-feldspar (20%) with dynamically recrystallized multicrystalline pressure shadows mostly display clockwise rotation (Figs. 3*e*, 3*f*). The pressure shadows consist of feldspar with minor quartz subgrains displaying serrated to straight boundaries and dominant polygonal to elongate shapes similar to the feldspar and quartz grains within the mylonite matrix. New randomly oriented biotite (10%) surrounds porphyroclasts within a 500 μm-wide zone, in which new hornblende (trace, 5%) is also locally intergrown.

Veins

Hornblende–quartz–biotite–K-feldspar–titanite veins, vein networks, and blastesis halos occur sporadically within the mylonite. Two veins cutting zone 1 ultramylonite were sampled for $^{40}Ar/^{39}Ar$ dating (#7 and #9, Table 1). The mineral assemblage in both is medium to coarse grained, and some grains have inclusions and intergrowths. Sample #7 is from a folded quartz–biotite–feldspar–hornblende vein that crosscuts the C-foliation and has a halo of hornblende blastesis. New

Fig. 4. Photomicrographs from a K-feldspar–hornblende (Hb)–quartz–biotite–titanite (Ti) vein (sample site # 9, Fig. 2). (*a*) Overall view of intergrown hornblende and K-feldspar (plane polarized light, 15 × magnification). (*b*) Same view under crossed polars. (*c*) Close up of the central portion of Fig. 4*a* illustrating equilibrium textures under crossed polars at 50 × magnification. (*d*) Chains of titanite crystals as inclusions within K-feldspar (from centre of Fig. 4*b*, 50 × magnification, crossed polars). (*e*) Mats of coarse titanite intergrown with hornblende, epidote, and biotite near the edge of the vein. (*f*) Titanite grain exhibiting a clear central core rimmed with fibrous titanite (50 ×, crossed polars).

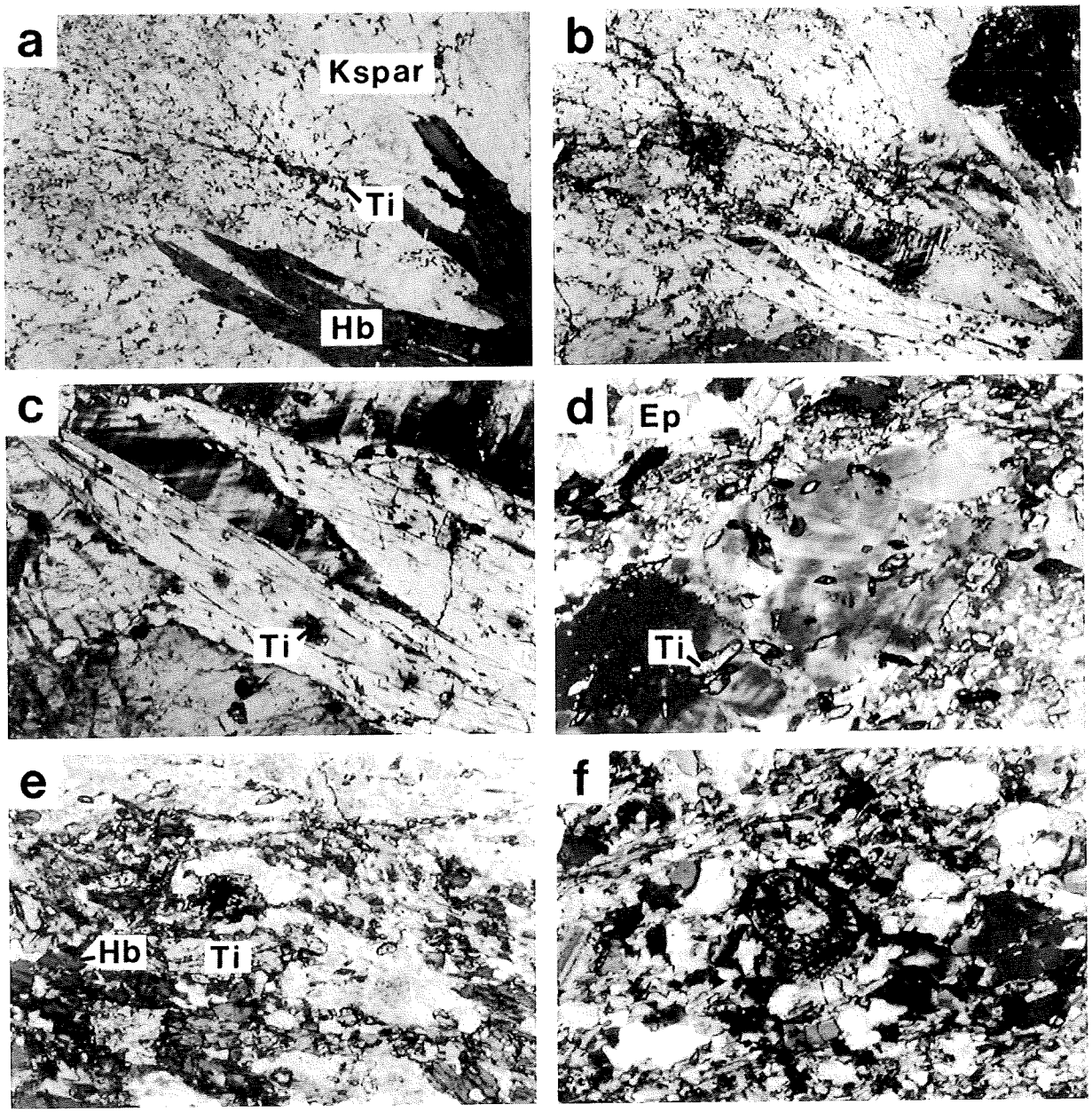

hornblende poikiloblasts (50–1500 μm) with faintly undulose extinction and tan to blue-green pleochroism occupy 20% modal of a 1 cm-wide zone surrounding the vein. They are rich in quartz, feldspar, and titanite inclusions that appear to have been enveloped during hornblende growth.

The vein represented by sample #9 exhibits a similar poikiloblastic hornblendic halo but is not folded. In this vein, large feldspar and hornblende grains share straight mutual grain boundaries (Figs. 4*a*, 4*b*). Randomly oriented titanite grains are locally abundant, particularly as inclusions within hornblende (Fig. 4*c*). Less common euhedral to subhedral titanite inclusions within K-feldspar (Fig. 4*d*) may represent trails precipitated during incremental feldspar growth. Irregular patches and zones of medium-grained titanite and hornblende intergrowth are present locally in some veins (Fig. 4*e*), and rare, zoned titanite grains occur within the mylonite; some of these have clear cores of titanite rimmed by concentric fibrous titanite crystals (Fig. 4*f*).

Analytical methods

Sample locations were chosen on the basis of the structural

database provided by Stauffer and Lewry (1993), and oriented samples were collected at key exposures with the aid of a rocksaw. Polished thin sections were cut in at least three orientations for each of the 24 candidate samples for geochronology. Ten samples were eventually selected for dating (Table 1), eight from the Needle Falls area, and two from a splay of the NFSZ in the Wathaman River area to the northeast, which was described by Lafrance and Varga (1996). Mineral separates were obtained from fresh unweathered material from 125–250 μm or 250–500 μm-size fractions by conventional mineral separation methods, including crushing, sieving, heavy liquids, Franz isodynamic separation, and hand picking using a binocular microscope. This yielded homogeneous mineral populations with at least 99% purity. A few grains from each mineral separate were mounted in a multihole block and analyzed by electron microprobe (EMP) using BSE to determine mineral homogeneity and to screen out any samples exhibiting pervasive mineral intergrowths.

Biotite grains from all samples were found to be clean, containing only rare traces of intergrown chlorite, representing much less than 1% by area, and were generally free of other inclusions or intergrowths. Hornblende grains contained minor quartz and titanite inclusions and rare traces of < 10 μm biotite intergrowths, which together represented < 0.1% by area. EMP selection of widely spaced points for individual analysis of major element oxide concentrations by WDS allowed further characterization of mineral composition and homogeneity (Table 2).

Procedures for stable isotope analysis at the University of Saskatchewan, Saskatoon, Saskatchewan, included extraction of oxygen from silicate minerals with BF_5 followed by quantitative conversion to CO_2 (Clayton and Mayeda 1963). Isotope abundances were measured on a Finnigan Mat 251 automated stable isotope mass spectrometer and are reported as values in per mil (‰) relative to Vienna standard mean ocean water (VSMOW). Working standards yielded 9.6‰ for the $\delta^{18}O$ value of U.S. National Bureau of Standards (NBS)-28 quartz and long-term reproducibilities average ± 0.2‰ 2σ (Table 1).

The $^{40}Ar/^{39}Ar$ incremental step heating, Ar extraction, and mass-spectrometric analyses were carried out at Queens University, Kingston, Ontario. Isotopic measurements were performed using a 180° MS-10 spectrometer, operated in the static mode. Linear regression of isotope ratios obtained for each step was carried out according to the procedures summarized by McDougall and Harrison (1988). Ages for each step were calculated using the decay constants recommended by Steiger and Jäger (1977). Decay constants were applied after corrections for background signal and irradiation-induced mass interferences. All ages and gas volumes are quoted with a 2 standard error estimate (±2σ) (Tables 1, 3).

Single-zircon Pb evaporation dating was carried out at the University of Saskatchewan to obtain the $^{207}Pb/^{206}Pb$ ages of zircons from two samples of mylonite by a modified version of the single-zircon Pb evaporation technique of Köber (1987) and Ansdell and Kyser (1991). Nonmagnetic, 125–250 μm diameter, subhedral–euhedral, translucent zircons were mounted directly on rhenium ionization filaments and resistance heated in steps. Pb isotope measurements were conducted using a Finnigan Mat 261 five-collector mass spectrometer in peak hopping mode, employing a secondary electron multiplier. Raw data were corrected using a mass fractionation factor of 0.11% per atomic mass unit. A diluted NBS982 Pb international reference standard was used as a calibration for all Pb isotopes. Incremental step heating of zircons provides a profile of the distribution of radiogenic Pb from the outer margins toward the center of the zircon (Ansdell and Kyser 1993). A series of high-temperature (1550–1620°C) steps that yield consistent Pb isotope ratios provides evidence of Pb homogeneity throughout the internal domains of the zircon suggesting no post-crystallization Pb loss. The highest temperature step is interpreted to represent the best estimate of the crystallization age of the zircon.

Titanite ages were obtained for two veins and one mylonite sample by conventional isotope extraction and thermal ionization mass spectrometry analytical procedures at the Geochronology Lab of the Geological Survey of Canada, Ottawa, Ontario (Tables 1, 4). Clear anhedral to subhedral grains were selected and strongly abraded. Multigrain analyses (3–4 grains) were necessary due to the low U concentration (Table 4). Regression lines were calculated, as described in Davis (1982).

Results

Microprobe analyses

Major-element oxide analyses were carried out for 12 samples (Table 2). Reproducibility of compositions obtained from widely spaced point analyses demonstrates reasonably good homogeneity. Biotite grains display minor variations in major elements, generally less than 10% between samples. On a biotite-composition diagram the analyses cluster about midway between the annite and phlogopite end members, with the tetrahedrally coordinated Al (Al_{IV}) close to 2.0 (Fig. 5*a*). Flourine concentrations range from 0.21–0.85 wt.%, signifying significant substitution of F^- for OH^-(Table 2). Amphiboles are compositionally uniform based on analyses of widely spaced points. Table 2 indicates that the amphibole grains are mostly edenite, spanning the edenite–hornblende boundary on an A-site (Na + K) vs. Si plot (Fig. 5*b*). As with the biotite grains, anomalous F was found in some of these samples, probably as a substitution within OH^- sites (Table 2).

Oxygen isotopes

In most samples, there is textural equilibrium in the assemblage hornblende–biotite–quartz–epidote–titanite–magnetite. Mineral pairs from nine samples were analyzed for oxygen isotopes to test for the conjunction of anion and textural equilibria (cf. Thompson 1987) and to determine the temperature at which the metamorphic minerals grew. Six quartz samples from NFSZ mylonites gave a relatively tight range of $\delta^{18}O$ from 8.7 to 10.0‰. Protomylonite in the hanging wall gave the lowest value of 6.8‰, whereas protolith Wathaman Batholith gave 9.6‰. Temperatures calculated for 19 mineral pairs based on relevant fractionation factors range from 430°C to 610°C, with a pronounced clustering at about 550°C (Fig. 6; Table 1; Chacko et al. 2001). Accordingly, retention of isotopic equilibrium of the quartz–hornblende and quartz–biotite pairs signify anion equilibrium, giving confidence that the $^{40}Ar/^{39}Ar$ plateaus represent the time of cooling through the respective blocking temperatures.

Table 2. Representative analyses of biotite, hornblende, and other minerals.

Mineral:	Biotite					Hornblende				K-feldspar	Albite	Titanite
Sample:	(5) #1	(6) #7	(8) #10	(8) #22	(6) #14	(7) #7	(8) #10	(6) #14	(3) #24	(5) #7	(3) #7	(1) #7
SiO_2 (wt.%)	37.26 ± 0.79	36.96 ± 0.33	38.30 ± 1.01	37.03 ± 0.88	36.47 ± 1.40	43.61 ± 0.44	44.42 ± 0.54	43.36 ± 0.76 0.76	44.92 ± 1.36	63.45 ± 0.64	66.39 ± 0.83	30.1
TiO_2	1.67 ± 0.07	1.92 ± 0.04	1.70 ± 0.12	2.29 ± 0.21	1.66 ± 0.11	0.82 ± 0.04	0.61 ± 0.06	1.01 ± 0.36	0.79 ± 0.37	0.03 ± 0.03	0.01 ± 0.01	36.98
Al_2O_3	14.68 ± 0.24	13.98 ± 0.22	14.76 ± 0.37	15.62 ± 0.31	14.76 ± 0.57	8.13 ± 0.22	8.66 ± 0.24	9.36 ± 0.37	9.11 ± 0.75	17.23 ± 0.24	18.91 ± 0.01	1.43
Cr_2O_3	0.02 ± 0.02	0.01 ± 0.01	0.05 ± 0.04	0.02 ± 0.02	0.02 ± 0.02	0.01 ± 0.02	0.03 ± 0.02	0.02 ± 0.02	0.03 ± 0.02	0.02 ± 0.02	0.02 ± 0.03	
FeO	18.04 ± 0.18	19.50 ± 0.11	16.33 ± 0.75	19.76 ± 0.62	17.00 ± 0.90	22.83 ± 0.32	19.20 ± 0.36	19.88 ± 0.26	19.55 ± 1.45	0.08 ± 0.07	0.12 ± 0.13	1.16
MgO	10.91 ± 0.43	10.75 ± 0.24	12.64 ± 0.31	8.78 ± 0.29	11.32 ± 1.33	8.42 ± 0.16	10.17 ± 0.38	9.71 ± 0.40	9.61 ± 0.96		0.02 ± 0.03	0.02
MnO	0.32 ± 0.02	0.23 ± 0.02	0.30 ± 0.04	0.35 ± 0.03	0.29 ± 0.07	0.30 ± 0.05	0.38 ± 0.03	0.42 ± 0.03	0.39 ± 0.04	0.03 ± 0.03		0.07
CaO	0.01 ± 0.02	0.01 ± 0.01	0.04 ± 0.03	0.02 ± 0.03	0.09 ± 0.13	11.42 ± 0.11	11.74 ± 0.12	11.6 ± 0.11	11.60 ± 0.23		0.69 ± 0.32	28.13
Na_2O	0.06 ± 0.01	0.04 ± 0.02	0.04 ± 0.02	0.06 ± 0.01	0.05 ± 0.01	1.29 ± 0.07	1.22 ± 0.08	1.38 ± 0.07	0.99 ± 0.06	0.41 ± 0.15	10.72 ± 0.27	
K_2O	9.40 ± 0.24	9.38 ± 0.07	9.42 ± 0.24	9.24 ± 0.31	8.83 ± 0.89	0.91 ± 0.05	0.85 ± 0.09	1.06 ± 0.15	0.79 ± 0.26	16.02 ± 0.22	0.15 ± 0.08	0.05
F	0.85 ± 0.07	0.55 ± 0.08	0.50 ± 0.05	0.27 ± 0.10	0.68 ± 0.36	0.23 ± 0.06	0.17 ± 0.07	0.09 ± 0.04	0.04 ± 0.03			0.68
Cl	0.07 ± 0.02	0.08 ± 0.04	0.09 ± 0.05	0.08 ± 0.04	0.09 ± 0.04	0.07 ± 0.04	0.05 ± 0.03	0.07 ± 0.04	0.05 ± 0.02	0.01 ± 0.02		
Total	93.29 ± 1.80	93.40 ± 0.45	94.15 ± 0.96	93.50 ± 1.42	91.23 ± 3.15	98.05 ± 0.36	97.49 ± 0.57	97.94 ± 0.42	97.87 ± 0.38	97.28 ± 0.71	97.05 ± 0.40	98.62
Atomic proportion												
Si	5.83	5.8	5.85	5.78	5.77	6.74	6.77	6.62	6.79			
Ti	0.2	0.23	0.2	0.27	0.21	0.01	0.07	0.12	0.09			
Al	2.71	2.59	2.66	2.87	2.77	1.48	1.55	1.68	1.62			
Cr	0	0	0.01	0	0	0	0	0	0			
Fe	2.36	2.56	2.08	2.58	2.29	2.95	2.45	2.54	2.47			
Mg	2.54	2.52	2.87	2.04	2.62	1.94	2.31	2.21	2.17			
Mn	0.04	0.03	0.04	0.05	0.04	0.04	0.05	0.05	0.05			
Ca	0	0	0.01	0	0.01	1.89	1.92	1.9	1.88			
Na	0.02	0.01	0.01	0.02	0.02	0.39	0.36	0.41	0.29			
K	1.88	1.88	1.83	1.84	1.8	0.18	0.17	0.21	0.15			
F	0.42	0.27	0.24	0.13	0.31	0.11	0.08	0.04	0.02			
Cl	0.02	0.02	0.02	0.02	0.03	0.02	0.01	0.02	0.01			
O	22	22	22	22	22	23	23	23	23			

Note: The number in brackets before the sample number is the number of analyses (*n*) carried out on that sample. Oxide wt.% is the average value among (*n*) consecutive point analyses with no points eliminated. STD, standard deviation. Fully automated Jeol JXA 8600 x-ray microanalyser using 5 μm diameter beam, 10 nA beam current, 15 Kv accelerating voltage. The following SPI™ mineral calibration standards were used: Si = diopside Ti = rutile, Al = kaersutite, Cr = chromite, Ca = bustamite, Mg = diopside, Na = jadite, *F* = fluorite, Cl = tugtapite, K = sanidine.

Fig. 5. (*a*) Composition of biotites summarized in a plot of Fe number vs. tetrahedrally coordinated Al. (*b*) Amphiboles plot across the edenite (hornblende) fields in a plot of A-site Na + K vs. Si (after Deer et al.1992).

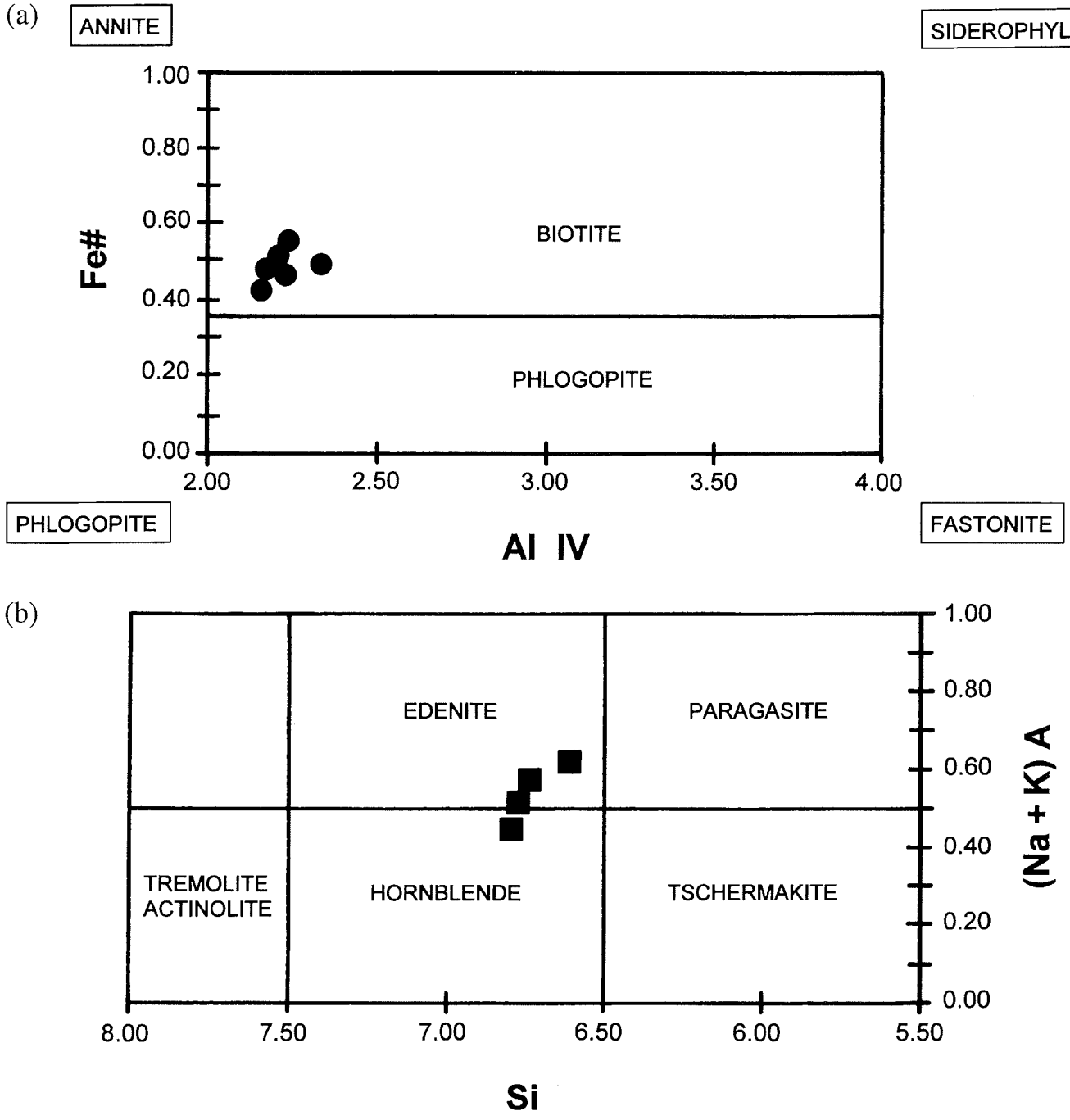

$^{207}Pb/^{206}$ Pb zircon ages

The oldest ages obtained from the highest temperature heating steps for zircons dated from each of two mylonite samples using the single-zircon Pb-evaporation technique are 1856 ± 3 and 1859 ± 4 Ma (Table 1), confirming that their protoliths were rocks of the Wathaman Batholith. The majority of published zircon dates for the Wathaman Batholith are between 1855 and 1860 Ma (Meyer et al. 1992). Younger ages of ~1844 to ~1809 Ma may be the result either of lead loss or zircon growth during metamorphism and deformation (Table 1). Peak thermal metamorphism and ductile deformation have been documented elsewhere in the THO between about 1840 and 1800 Ma (e.g., Ansdell and Norman 1995; Fedorowich et al. 1995; Sun et al. 1996).

$^{40}Ar/^{39}$ Ar ages

Fifteen hornblende and biotite samples were analyzed by conventional step-heating extraction and light-ion mass spectroscopy (Table 3). Twelve apparent plateau ages were obtained from the Needle Falls area and three from the Wathaman River area (Tables 1, 3; Fig. 7). The percentage of total ^{39}Ar represented by these plateaus is reported in Table 3,

Fig. 6. Histogram of temperatures obtained for 19 mineral pairs by stable isotope analyses and application of appropriate fractionation factors (Chacko et al. 2001; Table 1).

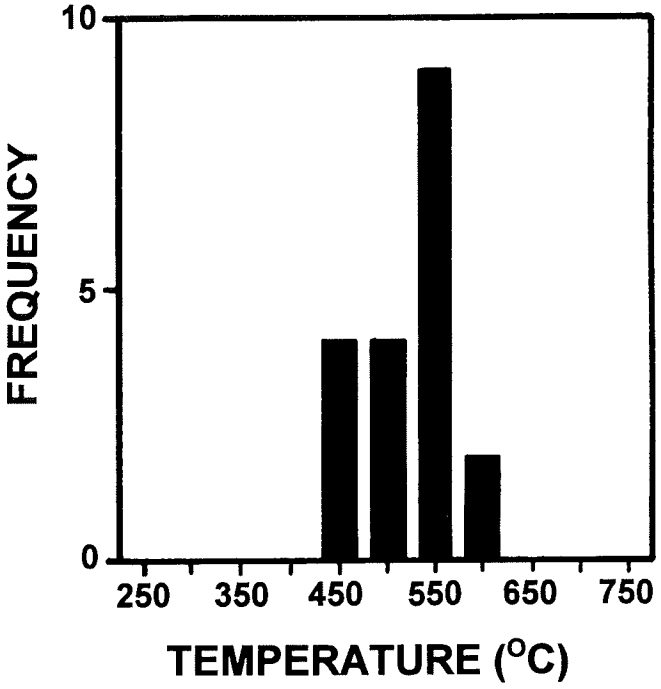

and the calculated correlation ages using the least-squares method suggested by York (1969) and Roddick (1978) are also shown for comparison. These isochrons compare well and are within the limits of analytical uncertainty of the plateau ages. By convention for the $^{40}Ar/^{39}Ar$ method, the plateau age is taken to represent the best estimate of the closure age for the sample through the mineral Ar blocking temperature.

Hornblende from three hornblende–biotite pairs in the Needle Falls area gave consistent ages that range from 1773 ± 11 to 1791 ± 7 Ma (Fig. 7; #7, zone 1 vein; #14, zone 3 mylonite; and #13, zone 4b protolith Wathaman Batholith). These ages are all within the 2σ analytical error of each other, and thus their average of 1780 ± 10 Ma is taken as the age at which hornblende cooled through its Ar blocking temperature of about 500°C (McDougall and Harrison 1988).

Biotite from these three hornblende-biotite pairs gave slightly younger ages, ranging from 1747 ± 8 to 1761 ± 7 Ma, with an average of 1757 ± 7 Ma, consistent with a blocking temperature of 300–350°C (McDougall and Harrison 1988; Freer 1981).

Three other, unpaired, plateau ages were also obtained (Table 3; Fig. 7). The 1772 ± 12 Ma hornblende age for #10 is within analytical error of those obtained from the three hornblende–biotite pairs previously discussed and supports the cooling age of 1780 ± 10 Ma. However, the 1738 ± 7 (Ma) (#1) and 1732 ± 9 Ma (#5) biotite ages are slightly younger, but are within 2σ analytical error of sample #13 (the youngest of the biotite ages obtained from hornblende–biotite pairs), perhaps indicating a wider time domain over which biotite cooled through its blocking temperature. The six remaining apparent plateau ages shown on Fig. 7 appear anomalously old.

Table 3. Summary of $^{40}Ar/^{39}Ar$ analytical data.

Sample	Mass (mg)	*J* value ± 2σ	Volume ^{39}Ar (cm^3)	~%K	~%Ca	Integrated age (Ma)	Correlation age (Ma)	MSWD	% ^{39}Ar	Plateau age (Ma)
NF area										
#1 — bi	10.0	0.035691 ± 0.000156	0.000000100	4.0	0.4	1732 ± 7	1744 ± 30	6.3	98.2	**1738 ± 7**
#5 — bi	6.0	0.035554 ± 0.000200	0.000000068	4.5	0.2	1720 ± 9	1746 ± 32	0.8	92.9	**1732 ± 9**
#7 — hb	23.0	0.035393 ± 0.000256	0.000000030	0.5	4.0	1811 ± 12	1772 ± 34	2.0	94.5	**1791 ± 7**
#7 — bi	9.8	0.035594 ± 0.000188	0.000000128	5.2	0.2	1743 ± 7	1720 ± 38	1.6	89.1	**1761 ± 7**
#9 — hb	27.0	0.035675 ± 0.000162	0.000000035	0.5	3.9	1879 ± 9	1816 ± 43	3.8	94.6	**1845 ± 9**
#10 — hb	15.0	0.035520 ± 0.000212	0.000000024	0.6	4.9	1781 ± 12	1776 ± 8	1.3	90.5	**1772 ± 12**
#13 — hb	27.0	0.035612 ± 0.000182	0.000000062	0.9	5.1	1790 ± 21	1773 ± 10	0.9	73.2	**1773 ± 11**
#13 — bi	10.2	0.035446 ± 0.000238	0.000000141	5.5	0.1	1739 ± 8	1746 ± 5	0.7	96.5	**1747 ± 8**
#14 — hb	30.0	0.035494 ± 0.000222	0.000000064	0.9	4.8	1782 ± 14	1774 ± 27	0.6	87.8	**1777 ± 11**
#14 — bi	8.7	0.035625 ± 0.000178	0.000000136	6.2	1.5	1737 ± 9	1737 ± 9	1.8	79.6	**1761 ± 7**
#16 — hb	23.0	0.035532 ± 0.000208	0.000000032	0.6	5.2	1884 ± 12	1884 ± 12	8.9	91.5	**1855 ± 10**
#16 — bi	8.0	0.035573 ± 0.000194	0.000000063	3.1	1.1	1905 ± 13	1905 ± 13	3.0	95.2	**1906 ± 12**
WR Area										
#22 — bi	10.5	0.035421 ± 0.000133	0.000000133	5.0	0.1	1792 ± 11	1792 ± 11	3.0	96.7	**1790 ± 11**
#24 — hb	30.0	0.035636 ± 0.000047	0.000000047	0.6	5.1	1914 ± 18	1914 ± 18	1.9	90.2	**1889 ± 18**
#24 — bi	10.0	0.035470 ± 0.000137	0.000000137	5.4	0.2	1890 ± 37	1890 ± 37	1.2	76.3	**1879 ± 9**

Note: All errors are calculated at twice standard error (2σ). Volumes are calculated at normal temperature and pressure. Approximate %Ca and %K are calculated from the measured $^{37}Ar/^{39}Ar$ ratios. MSWD, mean square weighted deviates.

Fig. 7. $^{40}Ar/^{39}Ar$ release spectra for three concordant hornblende and biotite pairs from a traverse across the NFSZ and its protoliths (see Table 3 for the analytical summary). Two unpaired biotites and one hornblende yielded similar plateau ages. Anomalously old plateau ages were obtained for another hornblende–biotite pair and an unpaired hornblende.

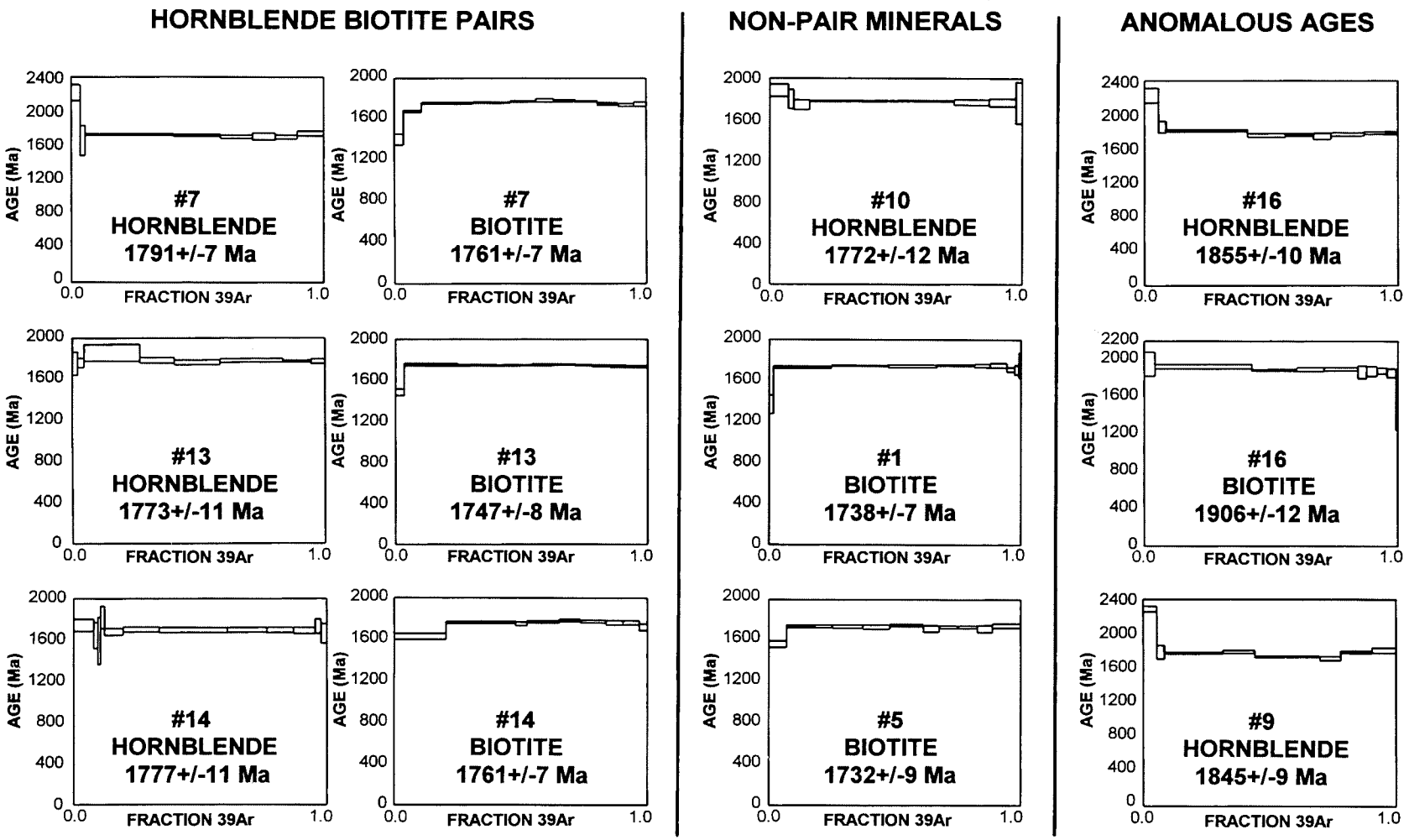

Table 4. Titanite U–Pb analytical data.

Titanite fraction	Wt. (mg)	U (ppm)	Pb (ppm)	$^{206}Pb/^{204}Pb$ [a]	Common Pb [a] (pg)	^{208}Pb [b] (%)	$^{206}Pb/^{238}U$ [c]	$^{207}Pb/^{235}U$	$^{207}Pb/^{206}Pb$ [c]	$^{207}Pb/^{206}Pb$ [d] Age (Ma)	D [e] (%)
#7	0.149	72	25	731	280	8.1	0.3273 ± 0.09%	5.281 ± 0.19%	0.11704 ± 0.14%	1912 ± 5	5.2
#9	0.14	62	19	350	457	5.3	0.3034 ± 0.12%	4.520 ± 0.37%	0.10803 ± 0.30%	1766 ± 11	3.7
#13	0.205	86	41	85	4921	32.0	0.3349 ± 0.44%	5.010 ± 1.80%	0.10850 ± 1.52%	1774 ± 55	–5.7

[a]Corrected for fractionation and spike.
[b]Radiogenic lead.
[c]Corrected for blank Pb and U and common Pb, errors are 1 standard error of the mean (%).
[d]Corrected for blank and common Pb, errors are 2 standard errors in Ma.
[e]Discordance; % of distance along discordia chord towards present day U/Pb ratios.

Titanite U–Pb ages

Three titanite samples were analyzed by the U–Pb method and yielded three different ages (Table 4; Fig. 8). Sample #9 yielded an age of 1766 ± 11 Ma, which is younger than the anomalous hornblende age obtained for this sample but is within the range of the normal hornblende and biotite plateau ages discussed in the preceding paragraphs (Table 1). Sample #7 gave an age of 1912 ± 5 Ma, which is much older than the normal hornblende and biotite plateau ages, and also ~55 Ma older than U–Pb zircon ages from the Wathaman Batholith (Meyer et al. 1992). The third titanite population (#13), which had high common lead, plots above concordia in Fig. 8 and is therefore uninterpretable.

Discussion of ages

Interpretation of Ar/Ar ages

The hornblende–biotite pairs from three variably strained parts of the NFSZ give ages that overlap within analytical uncertainty, and there is no significant difference between the ages of minerals from the mylonite and those from the younger crosscutting veins (Fig. 7). Samples #7 and #14 both represent new hornblende growth associated with K-feldspar–hornblende–biotite–quartz veins, whereas sample #13 is from megacrystic granitoid rocks of the Wathaman Batholith which exhibit local shear foliation and hornblende-biotite growth.

The three consistent hornblende ages for various zones of mylonites and veins across the deformed margin of the Wathaman Batholith indicate an estimated age for late- to posttectonic cooling through 500°C at 1780 ± 10 Ma. Biotite in the same samples yields a lower average plateau age of 1757 ± 7 Ma, consistent with retention of Ar at about 300–350°C. Younger biotite ages may be attributed to tectonic resetting, domainal diffusion effects, or a time spread for cooling through the biotite Ar retention temperature.

Several anomalous, older biotite and hornblende ages were also obtained. One hornblende–biotite pair from Needle Falls area zone 1 ultramylonite (#16) gave discordant, old plateau ages (1906 ± 12 Ma for biotite vs. 1757 ± 7 Ma for normal biotite and 1853 ± 10 Ma vs. 1780 ± 10 Ma for normal hornblende) and, unusually, an older age for biotite than for hornblende (Fig. 7; Tables 1, 3). Also, the biotite age is older than the Wathaman Batholith protolith from which the ultramylonite was derived (ca. 1857 Ma, Meyer et al. 1992). Another sample from the Needle Falls area, a vein cutting zone 1 ultramylonite derived from Wathaman Batholith material (#9), gave a hornblende plateau age of 1845 ± 9 Ma, about 65 Ma older than normal hornblende (Fig 7; Tables 1, 3). Also, mylonites from the Wathaman River study area, which are thought to have been derived from Wathaman Batholith protoliths, yielded a solitary biotite age of 1790 ± 11 Ma, more than 30 Ma older than the main population of biotites from the Needle Falls area (sample #22; Tables 1 and 3). Hornblende–biotite pair ages from sample #24 of 1889 ± 18 Ma and 1879 ± 9 Ma respectively, are more than 100 Ma older than normal hornblende and biotite, and considerably older than the Wathaman Batholith protolith (ca. 1857 Ma; Tables 1, 3).

These anomalous ages are attributed to excess Ar, the source of which is generally difficult to infer (McDougall

Fig. 8. Titanite concordia plot for separates. See Table 1 for sample details and Table 4 for the analytical summary.

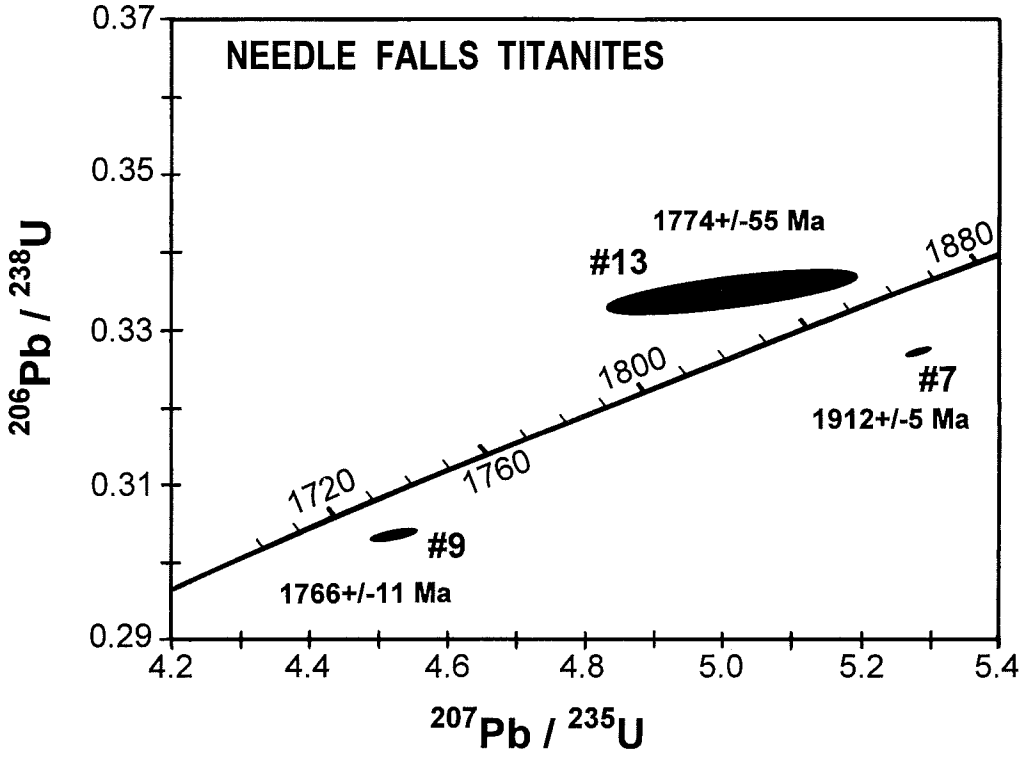

and Harrison 1988). It is probable that the source of excess Ar in the NFSZ samples could have been from fluids derived from deeper parts of the shear zone, where the rocks were still above the Ar retention temperature.

Interpretation of titanite ages

Given textural evidence for more than one generation of titanite, the scattered ages obtained are not unexpected and are difficult to interpret (Fig. 8). Only one titanite sample gave a possibly meaningful age (1766 ± 11 Ma), similar to the $^{40}Ar/^{39}Ar$ hornblende and biotite closure ages. The dispersed ages are consistent with the difficulties that other workers have had in using titanite to obtain metamorphic ages in medium to high-grade metamorphic terrains (e.g., Scott and St. Onge 1995). The problem may be diffusion of Pb through the titanite structure at elevated temperatures. One diffusion experiment for titanite indicates a Pb-blocking temperature range of between 460–600°C (Freer 1981), which is similar to the temperatures obtained by stable isotope geothermometry for the NFSZ (Fig. 6). Thus, the titanite ages obtained here may signify open-system behavior in the shear zone with respect to titanite Pb.

Summary

The textural associations of minerals in the NFSZ samples are key to understanding most of the ages. Preferred dimensional orientation of hornblende along the L-lineation, and of biotite along the C-foliation, indicates growth during deformation. Argon was not retained until about 1780 Ma, after the crosscutting veins were formed. This constrains the age of shearing and initial cooling to between 1857 Ma, the age of the Wathaman Batholith, and 1780 Ma, consistent with constraints on cooling to 500°C elsewhere in the Trans-Hudson Orogen (e.g., Ansdell and Norman 1995; Fedorowich et al. 1995; Sun et al. 1996). The hornblende blastesis and vein association indicate new growth of compositionally uniform hornblende, rather than a replacement of preexisting hornblende. Partially recrystallized hornblende and biotite might be expected to produce complex $^{40}Ar/^{39}Ar$ spectra without well-developed plateaus, which is not observed. The consistent population of biotite ages in both mylonite and veins indicates that cooling through ≤300°C did not occur until about 1757 Ma, after which no significant deformation took place along the NFSZ.

Implications and conclusions

The Needle Falls Shear Zone is a major orogen-parallel ductile high-strain zone in the Paleoproterozoic Trans-Hudson Orogen, in which the Hearne Province in the west was juxtaposed against the Wathaman Batholith (Stauffer and Lewry 1993). The NFSZ developed at temperatures of between 610°C and 500°C as constrained by the syntectonic metamorphic assemblage. Foliation, lineation, and fold orientations together indicate mainly dextral, oblique slip-shear displacement with a minor west-side-down component. Three concordant hornblende–biotite pair ages indicate that the NFSZ cooled through the hornblende blocking temperature of 500°C at 1780 ± 10 Ma and the biotite Ar blocking temperature of 300–350°C at 1757 ± 7 Ma, over an interval of ~23 million years, a rate of about 9°C/million years. If due entirely to post-orogenic uplift, which is uncertain, and a geothermal gradient of 30°C/km, this would indicate an average uplift of about 0.3 mm/year.

Regionally, early stages of the Trans-Hudson Orogen

Fig. 9. Time chart for the Reindeer Zone, showing the relationships among volcanism, plutonism, deformation, metamorphism, and the Needle Falls Shear Zone. Dates reported by different authors for the time of peak thermal metamorphism vary from place to place; however, they are everywhere within the 1840–1800 Ma time range. Based mainly on Lewry et al. (1987), Ansdell et al. (1995), Fedorowich et al. (1995), Sun et al. (1996), Ansdell et al. (1999), Ashton et al. (1999), Lucas et al. (1996), and Ryan and Williams (1999).

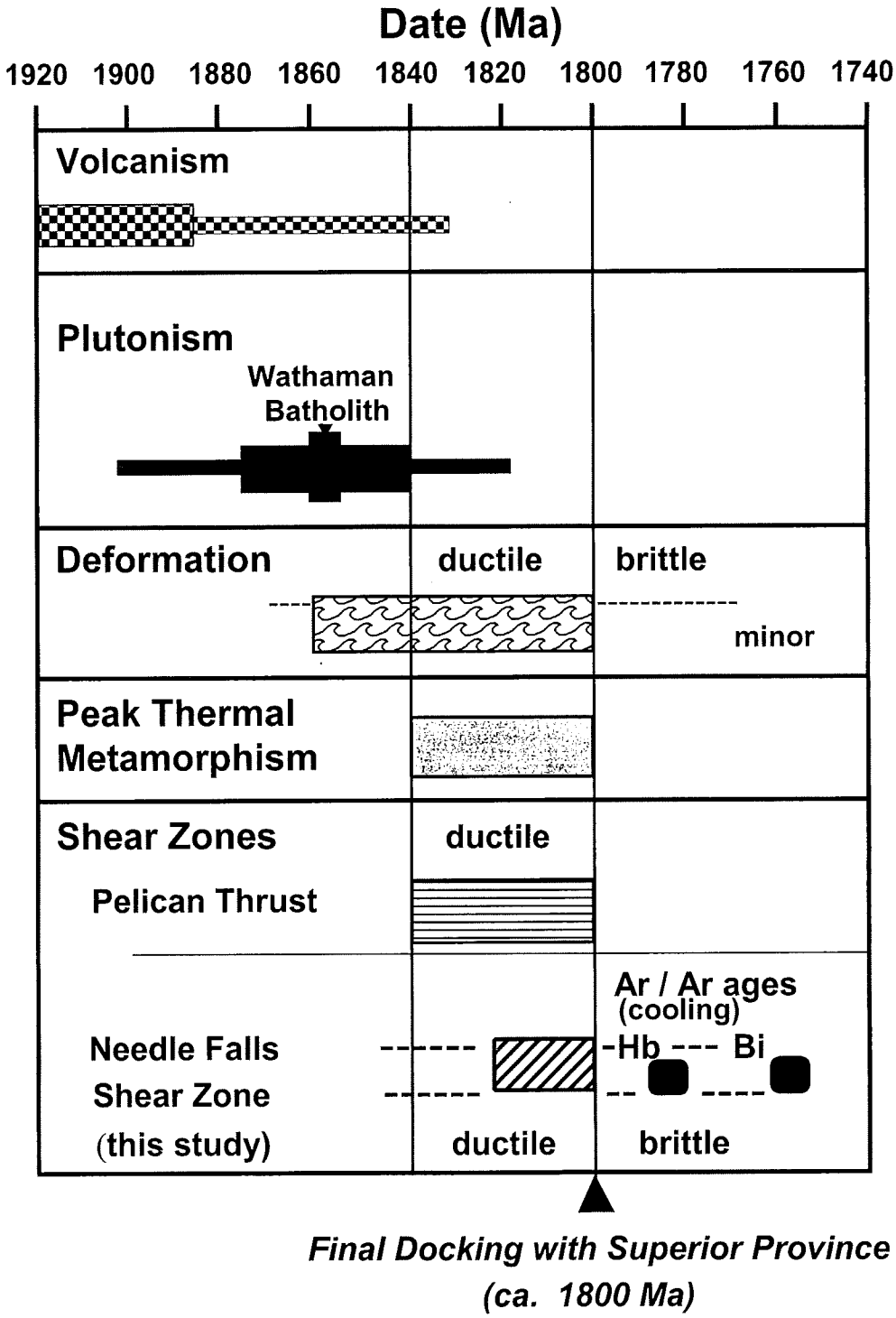

involved convergent margin arc magmatism during closure of the Manikewan Ocean, beginning about 1900 Ma (Stauffer 1984; Lucas et al. 1996; Fig. 9). The main phases of late- to post-collisional, ductile deformation, and peak thermal metamorphism occurred between about 1840 and 1800 Ma, although the timing may have varied somewhat locally (Fig. 9). The NFSZ was active mainly within the ductile regime; however, it cuts earlier ductile deformation features developed within the Wathaman Batholith, and thus was likely initiated after peak thermal metamorphic and ductile conditions were reached (Stauffer and Lewry 1993; Fig. 9). The NFSZ then cooled through 500°C prior to 1780 Ma,

consistent with the similar ductile–brittle transition that occurred in other parts of the Reindeer Zone to the east (Gordon 1989; Fedorowich et al. 1995; Marshall et al. 1997). One of the best-dated shear zones in the THO is the Pelican Thrust, a major ductile shear zone that appears to have been active for most of the 1840–1800 Ma time period (Ashton et al. 1999; Sun et al. 1996). The timing of movement on the NFSZ appears to have overlapped that of the Pelican Thrust, and they appear to have gone through the ductile–brittle transition at about the same time (~1800 Ma) (Fig. 9).

Acknowledgments

This research was carried out with the support of a Lithoprobe Research Grant to Rob Kerrich and Mel Stauffer. Steve Lucas of the Geological Survey of Canada is thanked for both logistical support in carrying out the fieldwork and for funding the titanite U–Pb analyses. Various others are to be thanked for their contributions, including: Kevin Ansdell, Doug Archibald, Tom Bonli, Jerry Grant, Ann Kinsman, Amabel Ortega, and Fried Schwerdtner. This paper has been improved from incisive critiques of two journal reviewers, K. Ashton and J. Ryan, and Associate Editor, Marc St. Onge.

One of the co-authors, Dr. John F. Lewry, died during the preparation of this paper. The remaining authors acknowledge John's contribution and appreciate his insights on the development of the Trans-Hudson Orogen.

References

Ansdell, K.M., and Kyser, T.K. 1991. Plutonism, deformation, and metamorphism in the Proterozoic Flin Flon greenstone belt, Canada: Limits on timing provided by the single-zircon Pb-evaporation technique. Geology, **19**: 518–521, 1991.

Ansdell, K.M., and Kyser, T.K. 1993. Textural and chemical changes undergone by zircon during the Pb-evaporation technique. American Mineralogist, **78**: 36–41.

Ansdell, K.M., and Norman, A.R. 1995. U–Pb geochronology and tectonic development of the southern flank of the Kisseynew Domain, Trans-Hudson Orogen, Canada. Precambrian Research, **72**: 147–167.

Ansdell, K.M., Lucas, S., Conners, K., and Stern, R.A. 1995. Kisseynew metasedimentary gneiss belt, Trans-Hudson orogen (Canada): Back-arc origin and collisional inversion. Geology, **23**: 1039–1043.

Ansdell, K.M., Conners, K.A., Stern, R., and Lucas, S. 1999. Coeval sedimentation, magmatism, and fold-thrust development in the Trans-Hudson Orogen: geochronological evidence from the Wekusko Lake area, Manitoba, Canada. Canadian Journal of Earth Sciences, **36**: 293–312.

Ashton, K.E., Heaman, L.M., Lewry, J.F., Hartlaub, R.P., and Shi, R. 1999. Age and origin of the Jan Lake Complex: a glimpse at the buried Archean craton of the Trans-Hudson Orogen. Canadian Journal of Earth Sciences, **36**: 185–208.

Bickford, M.E., Collerson, K.D., Lewry, J.F., Van Schmus, W.R., and Chiarenzelli, J.R. 1990. Proterozoic collisional tectonism in the Trans-Hudson orogen, Saskatchewan. Geology, **18**: 14–18.

Bottinga, Y., and Javoy M. 1975. Oxygen isotope partitioning among the minerals in igneous and metamorphic rocks. Reviews of Geophysics and Space Physics, **13**: 401–418.

Brodie, K.H., and Rutter, E.H. 1985. On the relationship between deformation and metamorphism, with special reference to the behavior of basic rocks. *In* Advances in physical geochemistry. *Edited by* A.B. Thompson and D.C. Rubie. pp. 139–179.

Clayton, R.N., and. Mayeda, T.K. 1963. The use of bromine pentafluoride in the extraction of oxygen from oxides and silicates for isotopic analyses. Geochimica Cosmochimica Acta, **27**: 43–52.

Chacko, T., Cole, D.K., and Horita, J. 2001. Equilibrium oxygen, hydrogen and carbon isotope fractionation factors applicable to geologic systems. Reviews in Mineralogy and Geochemistry, **43**: 1–61.

Davis, D.W. 1982. Optimum linear regression and error estimation applied to linear regression data. Canadian Journal of Earth Sciences, **19**: 2141–2149.

Deer, W.A., Howie, R.A., and Zussman, J. 1992. An Introduction to the Rock-Forming Minerals. Longman Scientific and Technical, Hong Kong.

Fedorowich, J.S., Kerrich, R., and Stauffer, M.R. 1995. Geodynamic evolution and thermal history of the central Flin Flon Domain, Trans-Hudson Orogen: Constraints from structural development, $^{40}Ar/^{39}Ar$, and stable isotope geothermometry. Tectonics, **14**: 472–503.

Freer, R. 1981. Diffusion in silicate minerals and glasses: a data digest and guide to the literature. Contributions to Mineralogy and Petrology, **76**: 440–454.

Gordon, T.M. 1989. Thermal evolution of the Kisseynew sedimentary gneiss belt, Manitoba: Metamorphism at an early Proterozoic accretionary margin. *In* Evolution of metamophic belts. *Edited by* J.S. Daly, R.A. Cliff, and B.W.D. Yardley. Geological Society of London, Special Paper 43, pp. 233–243.

Gromet, L.P. 1991. Direct dating of deformational fabrics. *In* Applications of radiogenic isotope systems to problems in geology. *Edited by* L. Heaman and J.N. Ludden. Mineralogical Association of Canada, Short Course Handbook 19, pp. 167–189.

Hajnal, Z., Lucas, S., White, D., Lewry, J., Bezdan, S., Stauffer, M.R., and Thomas, M.O. 1996. Seismic reflection images of high-angle faults and linked detachments in the Trans-Hudson Orogen. Tectonics, **15**: 427–439.

Jones, A.G., Craven, J.A., Ferguson, I.J., Boyce, T., Farquarson, C., and Ellis, R.G. 1993. North American Central Plains conductivity anomaly within the Trans-Hudson orogen in northern Saskatchewan, Canada. Geology, **21**: 1027–1030.

Kerrich, R., and Cassidy, K.F. 1994. Temporal relationships of lode gold mineralization to accretion, magmatism, metmorphism and deformation — Archean to present: A review. Ore Geology Reviews, **9**: 263–310.

Köber, B. 1987. Single grain evaporation combined with Pb^+ emitter bedding for $^{207}Pb/^{206}Pb$-age investigations using thermal ion mass spectrometry, and implications for zirconology. Contributions to Mineralogy and Petrology, **96**: 63–71.

Lafrance, B., and Varga, M. 1996. Structural studies of the Parker Lake Shear Zone and the Reilly Lake Shear Zone, Reindeer Lake. *In* Summary of investigations 1996. Saskatchewan Geological Survey, Saskatchewan Energy and Mines, Miscellaneous Report 96-4, pp. 119–124.

Lewry, J.F., and Collerson, K.D. 1990. The Trans-Hudson Orogen: extent, subdivision, and problems. *In* The early Proterozoic Trans-Hudson Orogen of North America. *Edited by* J.F. Lewry and M.R Stauffer. Geological Association of Canada, Special Paper 37, pp. 1–14.

Lewry, J.F., Macdonald, R., Livesy, C. Meyer, M., Van Schmus, R., and Bickford, M.E. 1987. U–Pb geochronology of accreted terranes in the Trans-Hudson Orogen, Northern Saskatchewan, Canada. *In* Geochemistry and mineralization of Proterozoic volcanic suites. *Edited by* T.C. Pharaoh, R.D. Beckinsale, and D. Richard. Geological Society of London, Special Publication 33, pp. 147–166.

Lucas, S.B., Green, A., Hajnal, Z., White, D., Lewry, J.F., Ashton, K., Weber, W., and Clowes, R. 1993. Deep seismic profile across a Proterozoic collision zone; surprises at depth. Nature (London), **363**: 339–342.

Lucas, S.B., Stern, R.A., Syme, E.C., Reilly, B.A., and Thomas, D.J. 1996. Intraoceanic tectonics and the development of continental crust: 1.92–1.84 Ga evolution of the Flin Flon Belt, Canada. Bulletin of the Geological Society of America, **108**: 602–629.

Marshall, D., Conners, K., and Ansdell, K. 1997. Thermochronology of hornblende and biotite from the Wekusko Lake area, Flin Flon Domain, Trans-Hudson Orogen, Manitoba. *In* Radiogenic age and isotopic studies: Report 10. Geological Survey of Canada, Current Research 1997-F, pp. 89–100.

McDougall, I., and Harrison, T.M. 1988. Geochronology and Thermochronology by the $^{40}Ar/^{39}Ar$ Method. Oxford University Press, New York.

Meyer, M.T., Bickford, M.E., and Lewry, J.F. 1992. The Wathaman batholith: An early Proterozoic continental arc in the Trans-Hudson orogenic belt, Canada. Geological Society of America Bulletin **104**, pp. 1073–1085.

Passchier, C.W., and Trouw, R.A.J. 1996. Microtectonics. Springer-Verlag, Berlin, pp. 289.

Ramsay, J.G., and Huber, M.I. 1987. The techniques of modern structural geology: Vol. 2, folds and fractures. Academic Press, London.

Roddick, J.C. 1978. The application of isochron diagrams in $^{40}Ar/^{39}Ar$ dating: a discussion. Earth and Planetary Science Letters, **41**: 233–244.

Ryan, J.J., and Williams, P.F. 1999. Structural evolution of the eastern Amisk collage, Trans-Hudson Orogen, Manitoba. Canadian Journal of Earth Sciences, **36**: 251–273.

Scott, D.J., and St-Onge, M.R. 1995. Constraints on Pb closure temperature in titanite based on rocks from the Ungava orogen, Canada: Implications for U–Pb geochronology and P–T–t path determinations. Geology, **23**: 1123–1126.

Stauffer, M.R. 1984. Manikewan: an early Proterozoic ocean in central Canada, its igneous history and orogenic closure. Precambrian Research, **25**: 2021–2035.

Stauffer, M.R., and Lewry, J.F. 1988. Kinematic investigation of part of the Needle Falls shear zone. Saskatchewan Geological Survey Miscellaneous Report 88-4, pp. 156–160.

Stauffer, M.R., and Lewry, J.F. 1993. Regional setting and kinematic features of the Needle Falls shear zone, Trans-Hudson Orogen. Canadian Journal of Earth Sciences, **30**: 1338–1354.

Steiger, R.H., and Jäger, E. 1977. Subcommission on geochronology: Conventions on the use of decay constants in geo- and cosmochronology. Earth and Planetary Sciences Letters, **69**: 359–362.

Sun, M., Kyser, K., Stauffer, M., Kerrich, R., and Lewry, J. 1996. Constraints on the timing of crustal imbrication in the central Trans-Hudson Orogen from single-zircon $^{207}Pb/^{206}Pb$ ages of granitoid rocks from the Pelican thrust zone, Saskatchewan. Canadian Journal of Earth Sciences, **33**: 1638–1647.

Thompson, J.B. 1987. A simple thermodynamic model for grain interfaces: Some insights on nucleation, rock textures, and metamorphic differentiation. *In* Chemical transport in metasomatic processes. *Edited by* H.C. Helgeson Reidel. Norwell, Mass., pp. 169–188.

York, D. 1969. Least squares fitting of a straight line with correlated errors. Earth and Planetary Science Letters, **5**: 320–324.